Advances in Computational Design, *Vol. 5, No. 2 (2020) 147-175*
DOI: https://doi.org/10.12989/acd.2020.5.2.147

Two rectangular elements based on analytical functions

Mohammad Rezaiee-Pajand* and Arash Karimipour

Department of Civil Engineering, Ferdowsi University of Mashhad, Mashhad, Iran

(Received June 13, 2019, Revised October 26, 2019, Accepted January 8, 2020)

Abstract. To achieve appropriate stresses, two new rectangular elements are presented in this study. For reaching this aim, a complementary energy functional is used within an element for the analysis of plane problems. In this energy form, the Airy stress function will be used as a functional variable. Besides, some basic analytical solutions are found for the stress functions. These trial functions are matched with each element number of degrees of freedom, which leads to a number of equations with the anonymous constants. Subsequently, according to the principle of minimum complementary energy, the unknown constants can be expressed in terms of displacements. This system can be rewritten in terms of the nodal displacement. In this way, two new hybrid-rectangular triangular elements are formulated, which have 16 and 40 degrees of freedom. To validate the outcomes, extensive numerical studies are performed. All findings clearly demonstrate accuracies of structural displacements, as well as, stresses.

Keywords: rectangular element; hybrid element; plane problem; finite element method; airy stress function

Notation

AR8	Accurate rectangular element with 16 degrees of freedom	AR20	Accurate rectangular element with 40 degrees of freedom	V_C^*	Complementary energy along the element boundaries
Π_C^*	Complementary energy within the element	C	Elastic flexibility matrix	φ	Airy stress function
t	Thickness of the element	σ	Elemental stress vector	T	Surface force vector on the element boundaries
U	Displacement vector along element boundaries	q^e	Elemental nodal displacement vector	E	Young's modulus
μ	Poisson's ratio	EFEM	Energy finite element method	σ^T	Stress transposed vector
T^T	Surface traction force transposed vector	T_x	Surface traction force transposed vector is x-direction	T_y	Surface traction force transposed vector is y-direction
σ_x	Normal stress in x-direction	σ_y	Normal stress in y-direction	τ_{xy}	Shear stress
l and m	direction cosines of the outer normal	u_i	Nodal displacements in x-direction	v_i	Nodal displacements in y-direction
n	Number of analytical solution	S and M	Matrix expressions	$N_i^0(\xi_1.\xi_2.\xi_3)$	shape function
Γ_{ij}	Element edges				

*Corresponding author, Professor, E-mail: rezaiee@um.ac.ir

http://www.techno-press.org/?journal=acd&subpage=7 ISSN: 2383-8477 (Print), 2466-0523 (Online)

1. Introduction

A finite element method is an efficient tool for solving a great variety of structural bodies. Displacement techniques are the most common way to formulate a new element. The weakness of this scheme is giving inaccurate stresses. In the past decades, many types of research have improved the performance of elements. Fleck *et al*. indicated that the shear resistance was raised when the wire diameter decreases from 170 to 12 μm, in torsion behavior on the copper wires Fleck *et al*. (1994). Likewise, this occurred in the micro-indentation and micro-bend test (Wei *et al.* 2001 and Nix *et al.* 1998, Koiter 1964 and Toupin 1962). According to the obtained outcomes, the classical mechanical field was unsuitable for the micro-scale test. Therefore, it was concluded that these theories were better to be used for the micro-structures. On the other hand, the couple stress theory is one of the useful theories for studies of the couple stress/strain gradient phenomena. For example, Mindlin and Koiter (1964) and Toupin (1962) suggested new couple stress theory. In another study, Hutchinson and Fleck (1993) presented a new couple stress theory containing one material's characteristics. Furthermore, Yang *et al.* (2002) recommended symmetrical stress function, including the material's properties. In another study, Bell (1969) satisfied the continuousness conditions of displacements and the first derivatives concurrently. Nevertheless, nodal coordinates of the element usually required more than the first derivatives of the displacement.

Zervos *et al*. (2001) examined the scale effect by using fourth-order accuracy 18 degrees of freedom triangular plate element. Each node had six degrees of freedom, in this article. In another research, Papanicolopulos and Zervos (2009) formulated third-order accuracy 3D hexahedral element function with 64 degrees of freedom. In this study, each node had 8 displacement degrees of freedom. According to the obtained outcomes, their method could be used directly to the couple stress/strain gradient theory by creating four-node plane elements. Nonetheless, such elements are not appropriate for use in engineering purposes, because, it is difficult to satisfy the boundary conditions due to higher-order derivatives of the node parameters.

Berry and Balazs (1979) found an Airy function method appropriate for the Schrödinger's calculation for a free circumstance of the quantum mechanics. It should be mentioned that such an Airy function included infinite energy. Therefore, this could not be recognized experimentally. Siviloglou and Christodoulides (2007) proposed a model by using the analogy between the optical paraxial equation and the potential-free Schrödinger equation. For the first time, they presented the concept of finite-energy Airy beams (FEAB). In another research, these investigators performed the experiment test Cen *et al.* (2011a). Later, the FEAB was studied extensively (Cen *et al.* 2011b, Sergei *et al.* 2016 and Albocher *et al.* 2009). These exclusive structures controlled the spatial FEAB to the particular applications, such as, the laser filamentation (Cen *et al.* 2011c and Zhou and Cen 2015). In addition to spatial Airy beam, the time-based Airy pulse propagated with its acceleration resulting from a varying group velocity was introduced (Madeo *et al.* 2012 and Madeo *et al.* 2014). It should be added, FEM has various uses, including light bullets generation, super continuum generation, solution manipulation, solution self-frequency shift and etc. (Zienkiewicz *et al.* 2005, Lee *et al.* 1993, Taylor *et al.* 1976, Chen *et al.* 2010, Ooi *et al.* 2004, Long *et al.* 1999 Chen *et al.* 2004 and Rezaiee-Pajand and Karimipour 2019b).

In the structural analysis area, the standard 8-node isoparametric element (Q8) is one of the most generally used finite element models. So far, its performance has been systematically measured by researchers. Stricklin *et al.* (1977) presented some consequences of a cantilever beam modeled using inaccurate elements. Furthermore, they presented that Q8 element stiffened and

performed very bad in some cases. Lee and Bathe studied the different effects of some Serendipity (Q8, Q12) and Lagrangian (Q9, Q16) elements by using different inaccurate meshes. They found that the Lagrangian type elements had better stability in most cases. Taylor (1989) stated the same conclusion. Rajendran and Liew (2003) used two diverse arrays of shape as the trial and test functions. They created an 8-node element, US-QUAD8, with unsymmetric element stiffness matrix. According to this study, this element showed excellent behavior in solving several benchmark problems.

By using bivariate quadratic splines on triangulated quad angulations, Li and Wang (2006) recommended a new 8-node spline element. According to the reported obtained outcomes, very good results for some problems were achieved, which had a reasonably complex mathematical behavior. In 1999, Long *et al.* established a new natural coordinate system for constructions of the quadrilateral element. Later, three 8-node models, AQ8-I, AQ8-II and QACM8, were successfully developed by Soh *et al.* (2000) and Cen *et al.* (2007), respectively.

In the elements with all four straight edges, the interpolation functions for the displacement responses possessed the second-order completeness, in both areas and the Cartesian coordinates. All of these elements showed excellent behavior under the flexural condition, and they were insensitive to the mesh unfairness. On the contrary, when an element edge is curved, the mentioned second-order completeness will no longer exist. In this and some other studies, the variational principles are frequently considered as the theoretical base of the finite element method. Among the others, Washizu (1982), Chien (1980) and Hu (1984) presented some useful discussions on this topic.

Lin *et al.* (2019) presented an analytical solution for accurate estimation of stress and displacement fields. Their schemes were used in the analysis of the shallow tunnel. The mentioned method was based on the complex variable technique, and the discrete Fourier transform. Furthermore, a linear curve was proposed for calculating the external maximum loading and the maximum displacement of the member. stress and displacement were assumed to be continuous along the excavation line. According to the obtained outcomes, the accuracy of their scheme decreased as the spatial distance between the geomaterials and the excavation line increases. These investigators defined a 5% error zone for the solution. In another study, Gao and Zou (2017) proposed an analytical solution for two and three-dimensional nonlinear Burgers' equation. They defined these equations in both square and a cubic space domain. All the boundaries and initial conditions were considered. The analytical solution for the three-dimensional Burgers' equation was given by the quotient of two infinite series, which involved hypergeometric, exponential, trigonometric and power functions. According to the obtained results, the solutions could find shock wave occurrences for the large Reynolds numbers ($Re \geq 100$). This was a helpful tool for testing the numerical methods.

Luis and Muñoz (2017) proposed an analytical solution for calculating the displacements field resulted from the reservoir compaction, under arbitrary pressure changes. Two new elements were suggested in this research. The related formulations were established by using the complementary energy functional within an element for the analysis of plane problems. To obtain the accurate values, some elementary analytical solutions were allocated for the stress functions. In another research, Haitao *et al.* (2012) solved the Euler–Bernoulli beam under arbitrary dynamic loads by using finite element methods. They used the modal superposition method along with the finite element scheme. As a result, the natural frequencies and modal shape functions were achieved by daunting continuity at the contact between different components of the element. In another study, Zhaolin *et al.* (2018) analyzed the Euler–Bernoulli beams with axial force under high-frequency

vibration by using an energy finite element method (EFEM). For this aim, the energy density and energy intensity of the beam were presented. Furthermore, the relationship between the wavenumber and group velocity was determined. The effects of axial force on the energy density response and the limitations of EFEM were also discussed.

Hsu (2016) solved the Timoshenko beam under free vibration by using an enriched finite element method. For this purpose, Lobatto's functions were used in order to establish the presented method. This investigator concisely explored the shear locking in the static structural analysis. To show the power of the used function, the obtained results were compared with the other numerical schemes. In order to solve plane elasticity problems, Li *et al.* (2015) proposed a multi-scale finite element method. They suggested an approach for numerically finding the shape functions by using the corresponding homogeneous governing formulas. The linear, quadratic and cubic shape functions were finally achieved by recommending the suitable boundary conditions. The obtained outcomes indicated that the multi-scale finite element scheme had a projecting improvement in solving the classic problems. Recently, Rezaiee-Pajand and Karimipour (2019a) present three new triangular elements. In their investigation, a complementary energy functional is used within an element for the analysis of plane problems using the Airy stress function. To validate the results, extensive numerical studies are accomplished. The findings clearly demonstrate accuracies of structural displacements as well as stresses.

Hou *et al*. (2016) used FEM in order to determine the behaviour of a system under shock load. They examined the dynamic response of anew designed ultrasonic system under half-sine shock impulses to check the sensitivity of the motor to the shocks in different directions. FEM was conducted to gain the relative displacement of a key point of the system. Numerical results show that the maximum relative displacement is of system and the maximum stress is five orders smaller than the Young´s modulus of the piezo material. Narwariya *et al.* (2018) presented a new method for analyzing abstemiously thick symmetric cross-ply laminated composite plate using FEM. The eight noded shell 281 elements are used to analyze the orthotropic plates and consequences are gained so that the right choice can be made in applications such as aircrafts, rockets, missiles, etc. to decrease the vibration amplitudes. Initially the model response for orthotropic plate and harmonic response for isotropic plate is verified with the available literature. The results are in good agreement with the available literature. Numerical consequences for the natural frequency and harmonic response amplitude are presented. Effects of boundary conditions, thickness to width ratio and number of layers on natural frequency and harmonic response of the orthographic plates are also investigated. Vini and Daneshmand (2019) investigated the bonding properties fabricated by the asymmetric roll bonding techniques by using analytical solution. The asymmetric RB process was carried out with thickness reduction ratios of 10%, 20% and 30% and mismatch rolling speeds 1:1, 1:1.1 and 1:1.2, separately. For various experimental conditions, finite element simulation was used to model the deformation of bimetallic laminates. Specific attention was focused on the bonding strength and bonding quality of the interface between Al and Cu layers in the simulation and experiment. The optimization of mismatch rolling speed ratios was obtained for the improvement of the bond strength of bimetallic laminates during the asymmetric RB process. Ushio *et al.* (2019) used the elastoplastic FEM analysis for earthquake response for the field-bolt joints of a tower-crane mast.

It is essential to design for this possibility and to take the necessary measures on construction sites. So, they created a new hybrid-element model that not only expressed the detailed behavior of the site joints an earthquake but also suppressed any increase in the total calculation time and revealed its behavior through computer simulations.

This article presents two new rectangular elements for analyzing the plane problems. To establish the suggested formulation, a complementary energy functional is utilized within an element. In order to calculate more accurate stresses, the well-known Airy stress function is included in the new elements. To reach this aim, some basic analytical solutions are assigned for the stress functions. These trial answers have some unknown parameters, which can be calculated by the principle of minimum complementary energy. In this procedure, two novel hybrid-rectangular triangular elements are formulated. Authors' elements have 16 and 40 degrees of freedom. Several numerical examples are solved to verify elements' performances. It is found that the suggested formulations can lead to accurate structural displacements and stresses.

2. Energy functional for airy stress function

In the finite element method, the corresponding energy functional is written in the following form:

$$\Pi_C = \Pi_C^* + V_C^* = \frac{1}{2}\int\int_{A^e}^{1} \sigma^T C\sigma t dA - \int_{\Gamma}^{1} T^T \bar{U} t ds \tag{1}$$

Different parts of this equation are given by:

$$\Pi_C^* = \frac{1}{2}\int\int_{A^e}^{1} \sigma^T C\sigma t dA \tag{2}$$

$$V_C^* = -\int_{\Gamma}^{1} T^T \bar{U} t ds \tag{3}$$

$$\sigma = \begin{Bmatrix} \sigma_x \\ \sigma_y \\ \tau_{xy} \end{Bmatrix} \tag{4}$$

$$C = \frac{1}{E'}\begin{bmatrix} 1 & -\mu' & 0 \\ -\mu' & 1 & 0 \\ 0 & 0 & 2(1+\mu') \end{bmatrix} \tag{5}$$

$$T = \begin{Bmatrix} T_x \\ T_y \end{Bmatrix} \tag{6}$$

$$\bar{U} = \begin{Bmatrix} \bar{u} \\ \bar{v} \end{Bmatrix} \tag{7}$$

Where, Π_C^* and V_C^* are the corresponding energy within the element and along the element boundaries, respectively. Moreover, t, σ, T, U, C and σ^T are the thickness of the element, the stress vector, the surface traction force vector through the element boundaries, the displacement vector along element boundaries, the elastic flexibility matrix and the stress transposed vector, correspondingly. Also, T^T is the surface traction force transposed vector, and T_x and T_y are the surface traction forces transposed vector is x and y direction, respectively. Furthermore, in the

plane stress problems, $E' = E$, $\mu' = \mu$ and for the plane strain cases, $E' = E/(1-\mu^2)$ and $\mu' = \mu/(1-\mu)$. It should be reminded that E and μ are the Young's modulus and Poisson's ratio, respectively. For the plane problems, the Airy stress function, φ, the stress vector, σ , can be defined as follows:

$$\sigma = \begin{Bmatrix} \sigma_x \\ \sigma_y \\ \tau_{xy} \end{Bmatrix} = \begin{Bmatrix} \dfrac{\partial^2 \varphi}{\partial y^2} \\ \dfrac{\partial^2 \varphi}{\partial x^2} \\ -\dfrac{\partial^2 \varphi}{\partial x \partial y} \end{Bmatrix} = \tilde{R}(\varphi) \tag{8}$$

Where, σ_x, σ_y and τ_{xy} are the normal stress in x-direction, normal stress in y-direction a(9)nd the shear stress, respectively. Applying the direction cosines, the surface traction force vector through the element boundaries has the next formulas:

$$T = \begin{Bmatrix} T_x \\ T_y \end{Bmatrix} = \begin{bmatrix} l & 0 & m \\ 0 & m & l \end{bmatrix} \begin{Bmatrix} \sigma_x \\ \sigma_y \\ \tau_{xy} \end{Bmatrix} = L\tilde{R}(\varphi) \tag{9}$$

$$L = \begin{bmatrix} l & 0 & m \\ 0 & m & l \end{bmatrix} \tag{10}$$

Where, l and m are the direction cosines of the outer normal, n, in the element boundaries. By substituting equations (8) and (9) into equation (1), the corresponding energy functional can be found as:

$$\Pi_C = \Pi_C^* + V_C^* = \frac{1}{2}\int \int_{A^e}^{1} \tilde{R}(\varphi)^T C \tilde{R}(\varphi) t dA - \int_{\Gamma}^{1} (L\tilde{R}(\varphi))^T \bar{U} t ds \tag{11}$$

Different parts of the last relation have the following forms:

$$\Pi_C^* = \Pi_C^* = \frac{1}{2}\int \int_{A^e}^{1} \tilde{R}(\varphi)^T C \tilde{R}(\varphi) dA \tag{12}$$

$$V_C^* = -\int_{\Gamma}^{1} (L\tilde{R}(\varphi))^T t ds \tag{13}$$

According to the basic equations of the finite element method, the element formulation is performed by using the energy functional containing the Airy stress function.

3. Analytical solutions of the stress function

In the plane problems with nobody forces, the Airy stress function satisfies the following equation:

$$\nabla^4\varphi = \frac{\partial^4\varphi}{\partial y^4} + 2\frac{\partial^4\varphi}{\partial x^2\partial y^2} + \frac{\partial^4\varphi}{\partial x^4} \tag{14}$$

In order to choose appropriate trial functions for establishing a new element, the following principles should be taken into account:

(1) The basic analytical solutions of the stress function should be selected to include the terms from the lowest-order to the higher-order.

(2) The resulting stress fields should hold completeness in the Cartesian Coordinates.

In this research, two new hybrid-rectangular elements are formulated. One of them is an eight-node rectangular element, which is named AR8. As it is seen in Fig. 1, this element possesses eight nodes and sixteen degrees of freedom. The second recommended element, which is called AR20, has twenty nodes and forty degrees of freedom. According to Fig. 1, all the nodes are located in the element sides and corners. Furthermore, it should be mentioned that the edges of the elements are curved. These sorts of elements are recommended to study their convergence power to the exact solutions. According to the number of nodes and degrees of freedoms in the element, stress function can be obtained. Therefore, all stress function parameters are found and listed in Tables 1-2. It should be mentioned that two types of coordinate systems, which are illustrated in Fig. 1, are used in this research. One of them is the Cartesian Coordinates, and the other is the Area Coordinates.

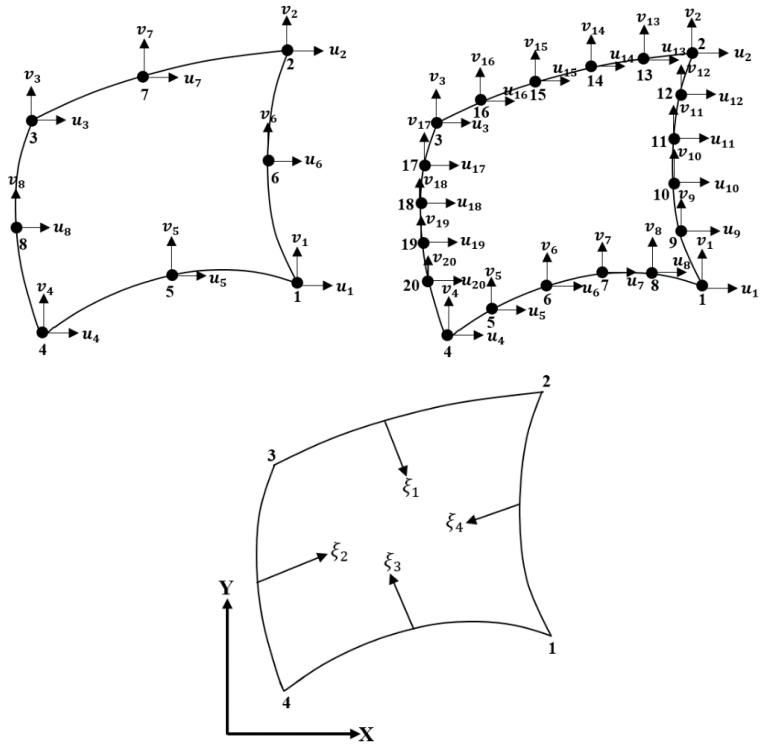

Fig. 1. Two proposed rectangular elements, AR8 and AR20

Table 1 Basic analytical solutions of stress function and stresses for AR8

	i	1	2	3	4	5	6	7	8
AR8	φ_i	$x+y$	xy	y^2	x^2	x^2+y^2	y^2x^2	x^2y+y^2x	x^3
	σ_x	0	0	2	0	2	$2x^2$	2x	0
	σ_y	0	0	0	2	2	$2y^2$	2y	6x
	τ_{xy}	0	-1	0	0	-x-y	-4xy	-2x-2y	0
	i	9	10	11	12	13	14	15	
	φ_i	y^3	x^3+xy^2	y^3+yx^2	y^4	x^3y	y^3x	y^4	
	σ_x	6y	2x	6y	$12y^2$	0	6xy	0	
	σ_y	0	6x	2y	0	6xy	0	$12x^2$	
	τ_{xy}	0	-2y	-2x	0	$-3x^2$	$-3y^2$	0	

4. Calculating the interpolation functions

At this stage, the degrees of freedom for the new elements are defined. According to Fig. 1, the element nodal displacement vector, q^e , for AR8 has the following shape:

$$q^e{}_8 = [u_1 \;\; v_1 \;\; u_2 \;\; v_2 \;\; u_3 \;\; v_3 \;\; u_4 \;\; v_4 \;\; u_5 \;\; v_5 \;\; u_6 \;\; v_6 \;\; u_7 \;\; v_7 \;\; u_8 \;\; v_8] \tag{15}$$

Similarly, the next nodal displacement can be written for AR20:

$$\begin{aligned} q^e{}_{20} = [&u_1 \;\; v_1 \;\; u_2 \;\; v_2 \;\; u_3 \;\; v_3 \;\; u_4 \;\; v_4 \;\; u_5 \;\; v_5 \;\; u_6 \;\; v_6 \; u_7 \; v_7 \;\; u_8 \;\; v_8 \;\; u_9 \;\; v_9 \;\; u_{10} \;\; v_{10} \\ &u_{11} \;\; v_{11} \;\; u_{12} \;\; v_{12} \;\; u_{13} \;\; v_{13} \;\; u_{14} \;\; v_{14} \;\; u_{15} \;\; v_{15} \;\; u_{16} \;\; v_{16} \;\; u_{17} \;\; v_{17} \;\; u_{18} \;\; v_{18} \;\; u_{19} \;\; v_{19} \;\; u_{20} \;\; v_{20}] \end{aligned} \tag{16}$$

Where, u_i and v_i are the nodal displacements, belong to the *x* and *y* directions. Based on these degrees of freedom, there are different analytical solutions for the stress function. All of them are presented in Tables 1 and 2. In the succeeding lines, the interpolation functions are established. For AR8, the next relationships are calculated and confirmed:

$$N_8 = \begin{Bmatrix} N_1 \\ N_2 \\ N_3 \\ N_4 \\ N_5 \\ N_6 \\ N_7 \\ N_8 \end{Bmatrix} = \begin{Bmatrix} -\frac{1}{4}(1+\xi_1\xi)(1+\eta_1\eta)(1-\xi_1\xi-\eta_1\eta) \\ -\frac{1}{4}(1+\xi_2\xi)(1+\eta_2\eta)(1-\xi_2\xi-\eta_2\eta) \\ -\frac{1}{4}(1+\xi_3\xi)(1+\eta_3\eta)(1-\xi_3\xi-\eta_3\eta) \\ -\frac{1}{4}(1+\xi_4\xi)(1+\eta_4\eta)(1-\xi_4\xi-\eta_4\eta) \\ \frac{1}{2}(1-\xi^2)(1-\eta_5\eta) \\ \frac{1}{2}(1-\eta^2)(1-\xi_6\xi) \\ \frac{1}{2}(1-\xi^2)(1-\eta_7\eta) \\ \frac{1}{2}(1-\eta^2)(1-\xi_8\xi) \end{Bmatrix} \tag{17}$$

Table 2 Basic analytical solutions of stress function and stresses for AR20

	i	1	2	3	4	5	6	7	8
	φ_i	x	y	x^2	xy	y^2	$-x^2-y^2$	x^3	$-x^2y$ $-xy^2$
	σ_x	0	0	0	0	2	-2	0	$-2x$
	σ_y	0	0	2	0	0	-2	$6x$	$-2y$
	τ_{xy}	0	0	0	1	0	$2x+2y$	0	$2x+2y$
	i	9	10	11	12	13	14	15	16
	φ_i	y^3	x^4	x^2y^2	$-x^3y-xy^3$	x^4	x^5	x^4y	xy^4
	σ_x	6y	0	$2x^2$	$-6xy$	0	0	0	$12xy^2$
	σ_y	0	$12x^2$	$2y^2$	$-6xy$	$12x^2$	$20x^3$	$12x^2y$	0
	τ_{xy}	0	0	$-4xy$	$3x^2+3y^2$	0	0	$-4x^3$	$-4x^3$
	i	17	18	19	20	21	22	23	24
	φ_i	y^5	$-x^3y^2$ $-x^2y^3$	x^6	x^5y	x^4y^2	$-x^3y^3$	x^2y^4	xy^5
	σ_x	$20y^3$	$-2yx^3$	0	0	$2x^4$	$-6yx^3$	$12x^2y^2$	$20xy^3$
	σ_y	0	$-6xy^2$ $-2y^3$	$30x^4$	$20x^3y$	$12x^2y^2$	$-6xy^3$	$2y^4$	0
AR20	τ_{xy}	0	$6x^2y$ $+6xy^2$	0	$5x^4$	$-8x^3y$	$9x^2y^2$	$-8xy^3$	$-5y^4$
	i	25	26	27	28	29	30	31	32
	φ_i	y^6	$-x^7$	x^6y	x^5y^2	$-x^4y^3$ $-x^3y^4$	x^2y^5	xy^6	$-y^7$
	σ_x	$30y^4$	0	0	$2x^5$	$-6x^4y$ $-12x^3y^2$	$20x^2y^3$	$30xy^4$	$-42y^5$
	σ_y	0	$-42x^5$	$30x^4y$	$20x^3y^2$	$-12x^2y^3$ $-6xy^4$	$2y^5$	0	0
	τ_{xy}	0	0	$-6x^5$	$-10x^4y$	$12x^3y^2$ $+12x^2y^3$	$-10xy^4$	$-6y^5$	0
	i	33	34	35	36	37	38	39	
	φ_i	$-x^4y^2$ $-x^2y^4$	$-x^5y^2$ $-x^2y^5$	$-x^4y$ $-xy^4$	$-x^4y^3$ $+x^3y^3$ $-x^3y^4$	$-x^3y^2$ $+x^2y^2$ $-x^2y^3$	x^2y-xy $+xy^2$	$x^5y^2-x^4y^2-x^2y^4$ $+x^2y^5$	
	σ_x	$-2x^4$ $-12x^2y^2$	$-2x^5$ $-20x^2y^3$	$-12xy^2$	$-6yx^4$ $+6x^3y$ $-12x^3y^2$	$-2x^3$ $+2x^2$ $-6x^2y$	$2x$	$2x^5-2x^4-12x^2y^2$ $+20x^2y^3$	
	σ_y	$-12x^2y^2$ $-2y^4$	$-20x^3y^2$ $-2y^5$	$-12x^2y$	$-12x^2y^3$ $+6xy^3$ $-6xy^4$	$-6xy^2$ $+2y^2$ $-2y^3$	$2y$	$20x^3y^2-12x^2y^2$ $-2y^4+2y^5$	
	τ_{xy}	$8x^3y$ $+8xy^3$	$10x^4y9$ $+10xy^4$	$4x^3+4y^3$	$12x^3y^2$ $-9x^2y^2$ $+12x^2y^3$	$6x^2y$ $-4xy$ $+6xy^2$	$-2x-2y$	$-10x^4y+8x^3y$ $+8xy^3-10xy^4$	

Similarly, the following interpolation functions are belonged to AR20:

$$N_{20}=\begin{Bmatrix}N_1\\N_2\\N_3\\N_4\\N_5\\N_6\\N_7\\N_8\\N_9\\N_{10}\\N_{11}\\N_{12}\\N_{13}\\N_{14}\\N_{15}\\N_{16}\\N_{17}\\N_{18}\\N_{19}\\N_{20}\end{Bmatrix}=\begin{Bmatrix}\frac{1}{8}(1+\xi_1\xi)(1+\eta_1\eta)(1+\xi_1\eta_1)\\\frac{1}{8}(1+\xi_2\xi)(1+\eta_2\eta)(1+\xi_2\eta_2)\\\frac{1}{8}(1+\xi_3\xi)(1+\eta_3\eta)(1+\xi_3\eta_3)\\\frac{1}{8}(1+\xi_4\xi)(1+\eta_4\eta)(1+\xi_4\eta_4)\\\frac{1}{8}(1+\xi_5\xi)(1+\eta_5\eta)(1+\xi_5\eta_5)\\\frac{1}{8}(1+\xi_6\xi)(1+\eta_6\eta)(1+\xi_6\eta_6)\\\frac{1}{8}(1+\xi_7\xi)(1+\eta_7\eta)(1+\xi_7\eta_7)\\\frac{1}{8}(1+\xi_8\xi)(1+\eta_8\eta)(1+\xi_8\eta_8)\\\frac{1}{4}(1-\xi^2)(1+\eta_9\eta)(1+\xi_9\eta_9)\\\frac{1}{4}(1+\xi_{10}\xi)(1-\eta^2)(1+\xi_{10}\eta_{10})\\\frac{1}{4}(1-\xi^2)(1+\eta_{11}\eta)(1+\xi_{11}\eta_{11})\\\frac{1}{4}(1+\xi_{12}\xi)(1-\eta^2)(1+\xi_{12}\eta_{12})\\\frac{1}{4}(1-\xi^2)(1+\eta_{13}\eta)(1+\xi_{13}\eta_{13})\\\frac{1}{4}(1+\xi_{14}\xi)(1-\eta^2)(1+\xi_{14}\eta_{14})\\\frac{1}{4}(1-\xi^2)(1+\eta_{15}\eta)(1+\xi_{15}\eta_{15})\\\frac{1}{4}(1+\xi_{16}\xi)(1-\eta^2\xi^2)(1+\xi_{16}\eta_{16})\\\frac{1}{4}(1-\xi^2)(1+\eta_{17}\eta)(1+\xi_{17}\eta_{17})\\\frac{1}{4}(1+\xi_{18}\xi)(1-\eta^2\xi^2)(1+\xi_{18}\eta_{18})\\\frac{1}{4}(1-\xi^2)(1+\eta_{19}\eta)(1+\xi_{19}\eta_{19})\\\frac{1}{4}(1+\xi_{20}\xi)(1-\eta^2\xi^2)(1+\xi_{20}\eta_{20})\end{Bmatrix} \tag{18}$$

5. Establishing the new elements

At the first step, the Airy stress function can be defined in terms of unknown parameters. A general form of this function is as follows:

$$\varphi = \sum_{i=1}^{n} \varphi_i \beta_i \tag{19}$$

Where, n is the number of analytical solution, and the other parts are given below:

$$\varphi = [\varphi_1 \ \ \varphi_2 \ldots\ldots \ \varphi_n] \qquad and \qquad \beta = [\beta_1 \ \ \beta_2 \ldots\ldots \ \beta_n] \tag{20}$$

Here, φ_i (i=1-n) are the number of analytical solutions for the stress function and β_1 (i=1-n) (i ¼ 1-15) are the number of unknown constants. Upon substitution of Eq. (21) into Eq. (12), the subsequent equation will be achieved:

$$\Pi_C^* = \frac{1}{2}\beta^T M \beta \tag{21}$$

$$M = \int \int_{A^e}^{1} S^T C S t dA \tag{22}$$

Where, S and M are the matrix expressions. Having these matrices, the analysis will be achieved. After performing the required calculations, the next result for AR8 will be found:

$$S_8 = \begin{bmatrix} 0 & 0 & 2 & 0 & 2 & 2x^2 & 2\text{x} & 0 & 6\text{y} & 2\text{x} & 6\text{y} & 12y^2 & 0 \\ 0 & 0 & 0 & 2 & 2 & 2y^2 & 2\text{y} & 6\text{x} & 0 & 6\text{x} & 2\text{y} & 0 & 6\text{xy} \\ 0 & -1 & 0 & 0 & -x-y & -4\text{xy} & -2\text{x}-2\text{y} & 0 & 0 & -2\text{y} & -2\text{x} & 0 & -3x^2 \end{bmatrix} \begin{bmatrix} 6\text{xy} & 0 \\ 0 & 12x^2 \\ -3y^2 & 0 \end{bmatrix} \tag{23}$$

AR20 has the following formula:

$$S_{20} = \begin{bmatrix} 0 & 0 & 0 & 0 & 2 & -2 & 0 & -2x & 6\text{y} & 0 & 2x^2 \\ 0 & 0 & 2 & 0 & 0 & -2 & 6x & -2y & 0 & 12x^2 & 2y^2 \\ 0 & 0 & 0 & 1 & 0 & 2x+2y & 0 & 2x+2y & 0 & 0 & -4xy \end{bmatrix}$$

$$\begin{matrix} -6xy & 0 & 0 & 0 & 12xy^2 & 20y^3 & -2yx^3 & 0 & 0 \\ -6xy & 12x^2 & 20x^3 & 12x^2y & 0 & 0 & -6xy^2-2y^3 & 30x^4 & 20x^3y \\ 3x^2+3y^2 & 0 & 0 & -4x^3 & -4x^3 & 0 & 6x^2y+6xy^2 & 0 & 5x^4 \end{matrix}$$

$$\begin{bmatrix} 2x^4 & -6yx^3 & 12x^2y^2 & 20xy^3 & 30y^4 & 0 & 0 & 2x^5 & -6x^4y-12x^3y^2 \\ 12x^2y^2 & -6xy^3 & 2y^4 & 0 & 0 & -42x^5 & 30x^4y & 20x^3y^2 & -12x^2y^3-6xy^4 \\ -8x^3y & 9x^2y^2 & -8xy^3 & -5y^4 & 0 & 0 & -6x^5 & -10x^4y & 12x^3y^2+12x^2y^3 \end{bmatrix}$$

$$\begin{bmatrix} 20x^2y^3 & 30xy^4 & -42y^5 & -x^4y^2-x^2y^4 & -2x^5-20x^2y^3 & -12xy^2 \\ 2y^5 & 0 & 0 & -2x^4-12x^2y^2 & -20x^3y^2-2y^5 & -12x^2y \\ -10xy^4 & -6y^5 & 0 & 8x^3y+8xy^3 & 10x^4y9+10xy^4 & 4x^3+4y^3 \end{bmatrix} \tag{24}$$

$$\begin{bmatrix} -6yx^4+6x^3y-12x^3y^2 & -2x^3+2x^2-6x^2y & 2x & 2x^5-2x^4-12x^2y^2+20x^2y^3 \\ -12x^2y^3+6xy^3-6xy^4 & -6xy^2+2y^2-2y^3 & 2y & 20x^3y^2-12x^2y^2-2y^4+2y^5 \\ 12x^3y^2-9x^2y^2+12x^2y^3 & 6x^2y-4xy+6xy^2 & -2x-2y & -10x^4y+8x^3y+8xy^3-10xy^4 \end{bmatrix}$$

All authors' elements are the hybrid type and curved sided. Based on this fact, the next formula can be recognized:

$$x=\sum_{i=1}^{n} N_i^0(\xi_1.\xi_2.\xi_3)x_i\ .\ y=\sum_{i=1}^{n} N_i^0(\xi_1.\xi_2.\xi_3)y_i\ . \tag{25}$$

Here, (x_i,y_i) refer to the Cartesian coordinates of the node i and $N_i^0(\xi_1.\xi_2.\xi_3)$ is its shape function. Therefore, the matrix M can be written as follows:

$$M=\int_{-1}^{1}\int_{-1}^{1}\int_{-1}^{1} S(\xi_1.\xi_2.\xi_3)^T CS(\xi_1.\xi_2.\xi_3)t|j|d\xi_1 d\xi_2 d\xi_3 \tag{26}$$

Where, $|j|$ is the Jacobian determinant. Substitution of Equation (21) into Equation (13) yields:

$$V_C^*=-\beta^T Hq^e \tag{27}$$

$$H=\int_{\Gamma}^{1} S^T L^T \bar{N} t dS \tag{28}$$

Matrices, $\bar{N}$ and H can be obtained according to the below relationships:

$$\bar{N}_8=\begin{bmatrix} N_1^0 & 0 & N_2^0 & 0 & N_3^0 & 0 & N_4^0 & 0 & N_5^0 & 0 & N_6^0 & 0 & N_7^0 & 0 \\ 0 & N_1^0 & 0 & N_2^0 & 0 & N_3^0 & 0 & N_4^0 & 0 & N_5^0 & 0 & N_6^0 & 0 & N_7^0 \end{bmatrix} \begin{bmatrix} N_8^0 & 0 \\ 0 & N_8^0 \end{bmatrix} \tag{29}$$

$$\bar{N}_{20}=\begin{bmatrix} N_1^0 & 0 & N_2^0 & 0 & N_3^0 & 0 & N_4^0 & 0 & N_5^0 & 0 & N_6^0 & 0 & N_7^0 & 0 \\ 0 & N_1^0 & 0 & N_2^0 & 0 & N_3^0 & 0 & N_4^0 & 0 & N_5^0 & 0 & N_6^0 & 0 & N_7^0 \end{bmatrix} \begin{bmatrix} N_8^0 & 0 & N_9^0 & 0 & N_{10}^0 & 0 & N_{11}^0 & 0 & N_{12}^0 & 0 & N_{13}^0 & 0 & N_{14}^0 & 0 \\ 0 & N_8^0 & 0 & N_9^0 & 0 & N_{10}^0 & 0 & N_{11}^0 & 0 & N_{12}^0 & 0 & N_{13}^0 & 0 & N_{14}^0 \end{bmatrix} \begin{bmatrix} N_{15}^0 & 0 & N_{16}^0 & 0 & N_{17}^0 & 0 & N_{18}^0 & 0 & N_{19}^0 & 0 & N_{20}^0 & 0 \\ 0 & N_{15}^0 & 0 & N_{16}^0 & 0 & N_{17}^0 & 0 & N_{18}^0 & 0 & N_{19}^0 & 0 & N_{20}^0 \end{bmatrix} \tag{30}$$

H can be written in the next form:

$$H=\int_{\Gamma_{ij}}^{1} S^T L^T \bar{N} t ds+\int_{\Gamma_{jk}}^{1} S^T L^T \bar{N} t ds+\int_{\Gamma_{kl}}^{1} S^T L^T \bar{N} t ds \tag{31}$$

Where, Γ_{ij}, Γ_{jk} and Γ_{kl} denote the element edges. The direction cosines of the outer normal of each element edge, l and m, can be expressed as follows:

$$l = \frac{dy}{ds} \ . \ m = -\frac{dx}{ds} \tag{32}$$

By inserting Eq (21) and (28) into Eq (11), the consequent element complementary energy function can be found:

$$\Pi_C^* = \frac{1}{2}\beta^T M\beta - \beta^T H q^e \tag{33}$$

To establish elemental formulation, by using the principle of minimum complementary energy, Π_C should be minimized:

$$\frac{\partial \Pi_C}{\partial \beta} = 0 \tag{34}$$

After calculating the nodal displacement vector, q^e, the unknown constant vector, β , can be achieved by the next relation:

$$\beta = M^{-1}Hq^e \tag{35}$$

Substitution of Eq. (39) into (37) yields:

$$\Pi_C^* = \frac{1}{2}{q^e}^T K^* q^e \tag{36}$$

$$K^* = (M^{-1}H)^T H \tag{37}$$

In the last equation, matrix K* can be considered as the equivalent stiffness matrix. This matrix can be used in the way as the conventional finite element technique. After finding the element nodal displacement vector, q^e, the element stresses can be written as:

$$\sigma = SM^{-1}Hq^e \tag{38}$$

Having the stress function for each element, stresses at all points will be in hand. In fact, the stress value at any point within the element can be determined by inserting the Cartesian coordinates of that point into Eq. (42).

6. Steps of analysis

In order to determine the responses of a structure by using presented elements, the following steps should be employed:

1. The external boundary conations (supports and loads) should be determined.
2. The pattern of mesh (number of elements and nodes point) should be given.
3. The matrix of S should be calculated based on the presented values of function for different points (φ_i)
4. The value of H, which is based on the shape functionn(N_i), and the value of S, should be determined. It should be mentioned that the value of H is formed for the whole structure.
5. By using Eq. 38, the stress function, which is the function of the value of x and y, is determined. The boundary condition should be applied on the obtained function.
6. By inserting the value of different points, the value of stresses in each coordinate should be calculated.

7. The strain values should be calculated by using the stiffness matrix and the stress matrix.
8. By using the integration of the strain matrix, the matrix of displacement for the structure should be calculated.

7. Numerical examples

Ten different problems are considered to assess the performance of the two new elements. To perform a widespread study, the presented formulations are used in authors' program. The obtained outcomes by this program are compared with the well-known available reference Fu *et al.* (2010). Based on the numerical achieved values, required brief discussion will be given on the validity and efficiency of the suggested elements.

7.1 Example 1

A cantilever beam divided by two different elements, as shown in Fig. 2. In this example, the Poisson's ratio, modulus of elasticity and thickness are 0.25, 1×10^6 and 0.001, respectively. Furthermore, both pure bending, under moment, M, and the linear bending under transverse force, P, are considered, as an external loading. It should be mentioned that the loads are applied on the free end of the beam.

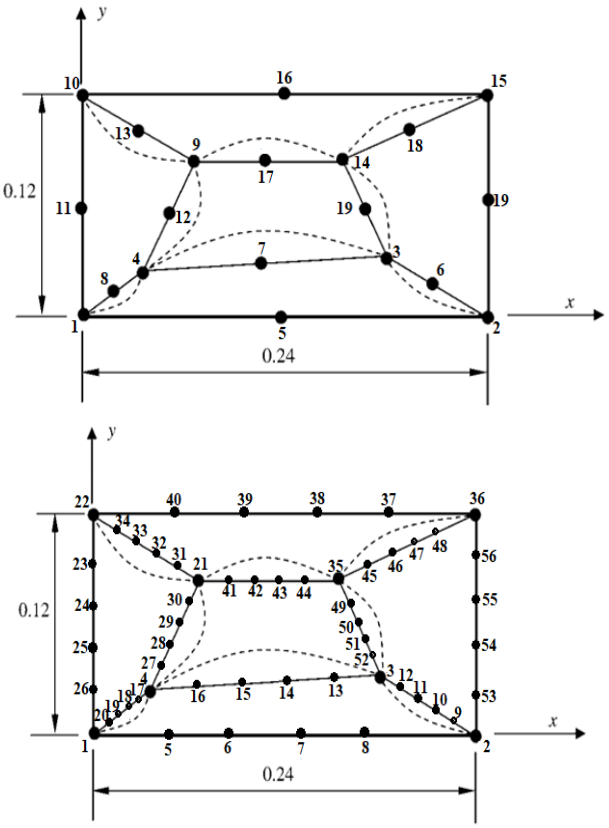

Fig. 2 Example 1 with different elements

In this example, the displacement outcomes corresponding to the constant strain case are calculated by the following equation:

$$u = 10^{-3}\left(\frac{x+y}{2}\right), \qquad u = 10^{-3}\left(\frac{y+x}{2}\right) \tag{39}$$

For this example, the exact stress response is given by:

$$\sigma_x = \sigma_y = 1333.3333 \quad , \quad \tau_{xy} = 400.0 \tag{40}$$

Displacement outcomes and the coordinate of nodes are represented in Table 3. It should be mentioned that these displacements belong to the boundary conditions. Additionally, the exact displacement results are shown in Table 2. These obtained answers demonstrate that the new elements have a suitable performance. In addition, all the outcomes exhibit that more accurate answers can be found by increasing the number of degrees of freedom.

Table 3 The coordinates and displacements of control nodes in the patch test

Coordinates		Elements	Nodes	Displacements $\times 10^{-3}$	
u_i	v_i			u_i	v_i
0.04	0.02	8-nodes element (Fu *et al.* 2010)	1	0.05	0.04
0.18	0.03		2	0.195	0.12
0.16	0.08		3	0.20	0.16
0.08	0.08		4	0.12	0.12
0.00	0.00		5	0.00	0.00
0.24	0.00		6	0.24	0.12
0.24	0.12		7	0.30	0.24
0.00	0.12		8	0.06	0.12
0.04	0.02	AR8	4	0.04	0.04
0.18	0.03		3	0.19	0.11
0.16	0.08		14	0.20	0.14
0.08	0.08		9	0.11	0.11
0.00	0.00		1	0.00	0.00
0.24	0.00		2	0.22	0.10
0.24	0.12		15	0.295	0.29
0.00	0.12		10	0.05	0.11
0.04	0.02	AR20	4	0.05	0.04
0.18	0.03		3	0.195	0.12
0.16	0.08		35	0.20	0.16
0.08	0.08		21	0.12	0.12
0.00	0.00		1	0.00	0.00
0.24	0.00		2	0.24	0.12
0.24	0.12		36	0.30	0.24
0.00	0.12		22	0.06	0.12

7.2 Example 2

As it is shown in Fig. 2, a cantilever wedge is under a uniformly distributed load q. Due to its triangular shape, the wedge is not easy to be divided by undistorted quadrilateral elements. The theoretical solutions for this problem are given by the following formula Cen *et al.* (2012):

$$\begin{cases} \sigma_r = \dfrac{q}{tan\alpha - \alpha}(\alpha - \theta - sin\theta cos\theta - sin^2\theta tan\alpha) \\ \sigma_\theta = \dfrac{q}{tan\alpha - \alpha}(\alpha - \theta + sin\theta cos\theta - cos^2\theta tan\alpha) \\ \tau_{r\theta} = \dfrac{q}{2(tan\alpha - \alpha)}(1 + sin^2\theta - cos^2\theta - 2tan\alpha sin\theta cos\theta) \end{cases} \tag{41}$$

In this example, the obtained outcomes with the different number of mesh are considered. Then, the analytical trial function method for developing an 8-node and 20-plane element suggested by Cen *et al*. (2012) is applied for the comparison purpose. The typical meshes are shown in Fig. 8. In this example, the Poisson's ratio, modulus of elasticity and thickness are 0.25, 1×10^7 and 0.1, respectively. It should be mentioned that P=1 for thin curved bar; and 100 for thick curved bar are distributed as $\tau_{xy} = -\frac{P}{N}\left[y + \frac{a^2b^2}{y^3} - \frac{1}{y}(a^2 + b^2)\right]$. In this formula, $N = a^2 - b^2 + (a^2 + b^2)log\frac{b}{a}$. The obtained results are presented in Table 4.

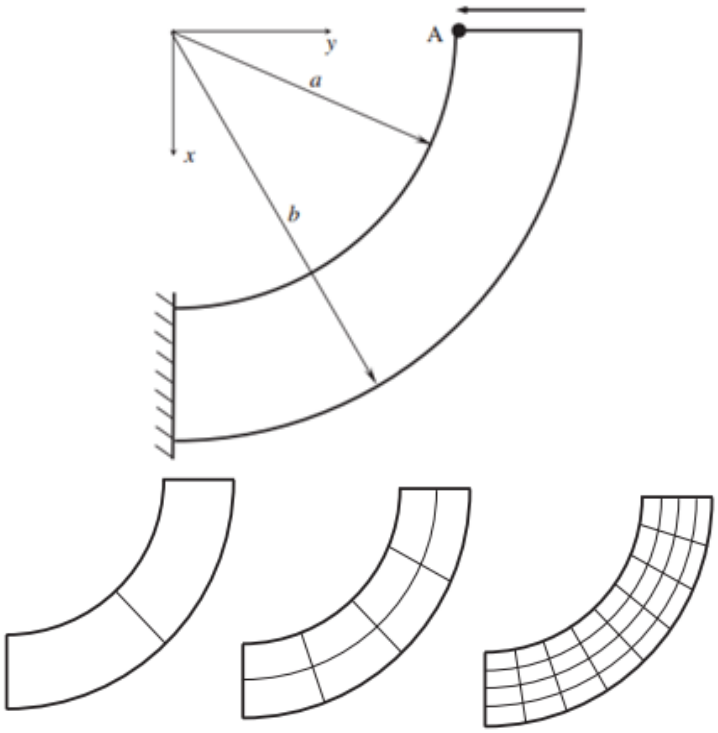

Meshes for thick curved bar: 1×2, 2×4 and 4×8

Fig. 3 Bending of a curved bar

Table 4 Normalized tip deflection at point A

Elements	Meshes		
	1×2	2×4	4×8
Q8 Cen *et al.* (2012)	0.6502	0.9587	0.9950
HSF-Q8 Cen *et al.* (2012)	0.9028	0.9834	0.9949
US-QUAD8 Cen *et al.* (2012)	0.7190	0.9615	0.9955
AR8	0.6724	0.9736	0.9999
AR20	0.914	0.9301	0.9358
Exact		0.936	

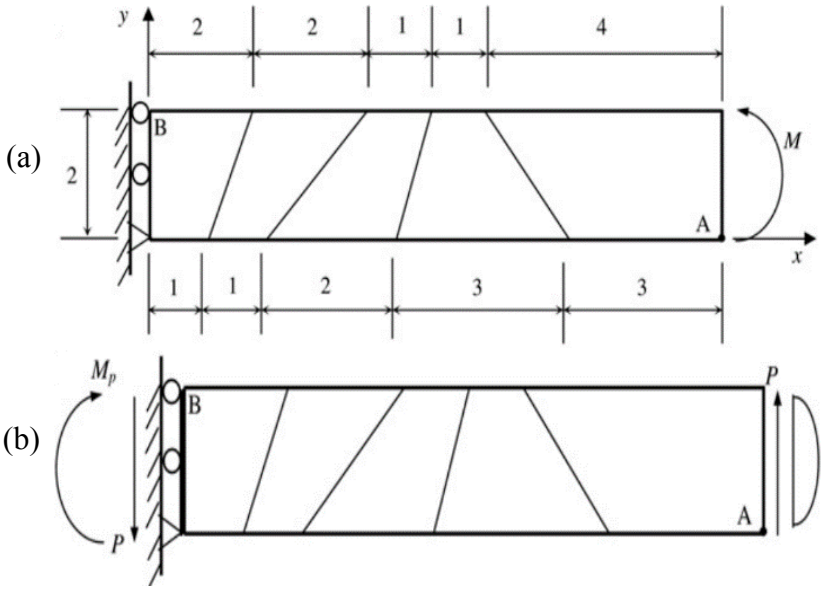

Fig. 4 Cantilever beam with different elements a) under pure bending b) under transverse load

7.3 Example 3

A cantilever beam is meshed with the different elements, as it is presented in Fig. 4. For this problem, two loading types are applied. The first one is pure bending, and the other type is bending under transverse force. In this figure, the numbers of nodes are not shown, but they are the same for all meshes.

In Fig. 4, a pure moment of $M = 2000$ is distributed as $f_x = -120y + 120$. Linear loading of $P = 300$ is distributed by $f_y = 75y - 37.5y^2$. Moreover, a moment of $M_P = 3000$ is distributed as $f_x = -180y + 180$. It should be added that the Young's modulus, Poisson's ratio and thickness of the structure are 1500, 0.25 and 10, respectively. The outcomes of the vertical deflection at the point A, (v_A), and the stress at the point B, (σ_{xB}), are given in Table 5. As it is seen in Table 5, both AR8 and AR20 have more accurate stress and displacement responses than the others.

Table 5 The displacement and stresses at selected at point A and B in Fig. 4

Element	Moment M		Load P	
	v_A	σ_{xB}	v_A	σ_{xB}
Q8 Fu *et al.* (2010)	99.7	-2984	101.5	-4422
QACM8 Fu *et al.* (2010)	101.3	-2920	102.8	-4320
ATF-Q8 Fu *et al.* (2010)	100.0	-3000	102.6	-4442
AR8	99.7	-2983	101.4	-4422
AR20	99.9	-2998	102.6	-4501
Exact	100.0	-3000	102.6	-4500

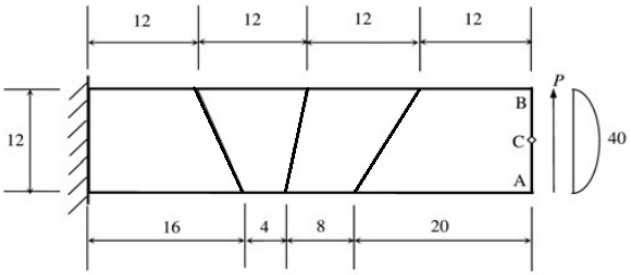

Fig. 5. Mesh for the cantilever beam

Table 6 The deflections at selected locations for bending problem of a cantilever beam

Element	Displacement			
	Point A	Pint B	Point C	Average
Q8 Fu *et al.* (2010)	0.3481	0.3474	0.3481	0.3479
QACM8 Fu *et al.* (2010)	0.3524	0.3517	0.3519	0.3520
ATF-Q8 Fu *et al.* (2010)	0.3567	0.3561	0.3558	0.3562
AR8	0.3479	0.3472	0.3481	0.3477
AR20	0.3557	0.3555	0.3559	0.3557
Exact	0.3558			

7.4 Example 4

In this part, a cantilever beam meshes as shown in Fig. 5. The displacement at points A, B and C are found and presented in Table 6. According to the obtained outcomes, new rectangular element, AR20, with 40 degrees of freedom gives the accurate values. In this example, E, μ and t are considered as 300000, 0.25 and 1.0, respectively. Furthermore, P is equal to 40 and is distributed by $f_y = \frac{5y}{3} - \frac{5y^2}{36}$.

7.5 Example 5

According to Fig. 7, a cantilever wedge is subjected to a uniformly distributed load q. Numerical results and the percentage errors of the radial stresses at the selected points are listed in

Table 5. Again, the presented element, AR20, performs very well for such a complex bending problem. In this example, E, μ and t are considered as 10000, 0.333 and 1.0, respectively. The theoretical solutions for this problem are available Fu *et al.* (2010):

$$\begin{cases} \sigma_r = \dfrac{q}{tan\alpha - \alpha}(\alpha - \theta - sin\theta cos\theta - sin^2\theta tan\alpha) \\ \sigma_\theta = \dfrac{q}{tan\alpha - \alpha}(\alpha - \theta + sin\theta cos\theta - cos^2\theta tan\alpha) \\ \tau_{r\theta} = \dfrac{q}{2(tan\alpha - \alpha)}(1 + sin^2\theta - cos^2\theta - 2tan\alpha sin\theta cos\theta) \end{cases} \tag{42}$$

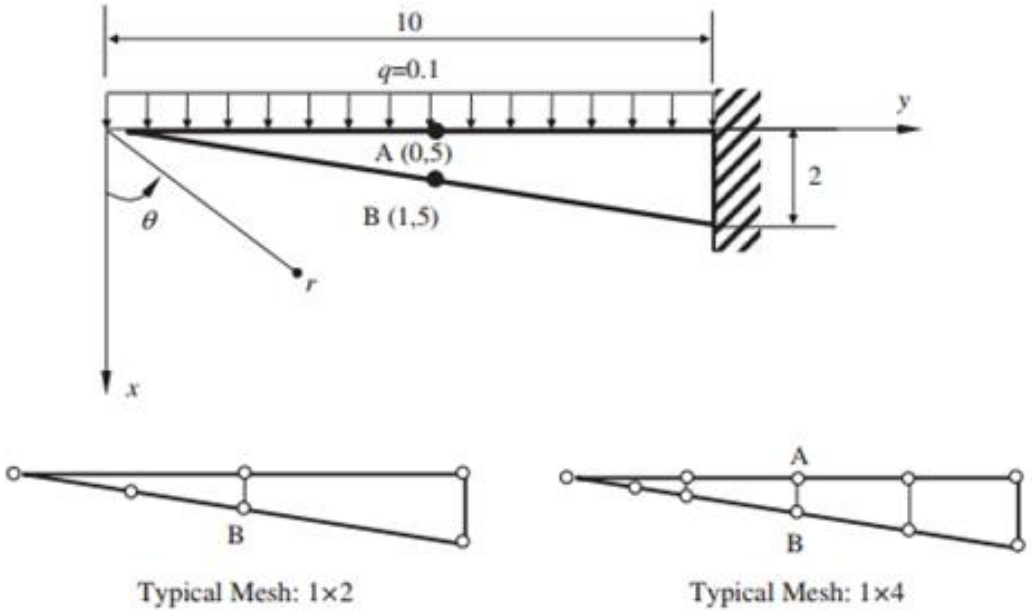

Fig. 6. A wedge subjected to a uniformly distributed load

Table 5 Results of radial stress at selected points for a wedge subjected to a uniformly distributed load

Mesh	σ_r at point A (0,5)			
	Cen *et al.*(2012)	AR8	AR20	Exact
1 × 6	7.6835 (1.38%)	7.6820 (1.35%)	7.5934 (0.19%)	
2 × 12	7.5894 (0.13%)	7.5835 (0.05%)	7.5812 (0.02%)	7.5792
4 × 24	7.5806(0.02%)	7.5805 (0.02%)	7.5794 (0.00%)	
	σ_r at point B (1,5)			
1 × 6	-7.7920 (1.47%)	-7.7512 (0.93%)	-7.7243 (0.58%)	
2 × 12	-7.7088 (0.39%)	-7.7021 (0.29%)	-7.7014 (0.28%)	-7.6792
4 × 24	-7.6832 (0.05)	-7.6805 (0.02%)	-7.6797 (0.00%)	

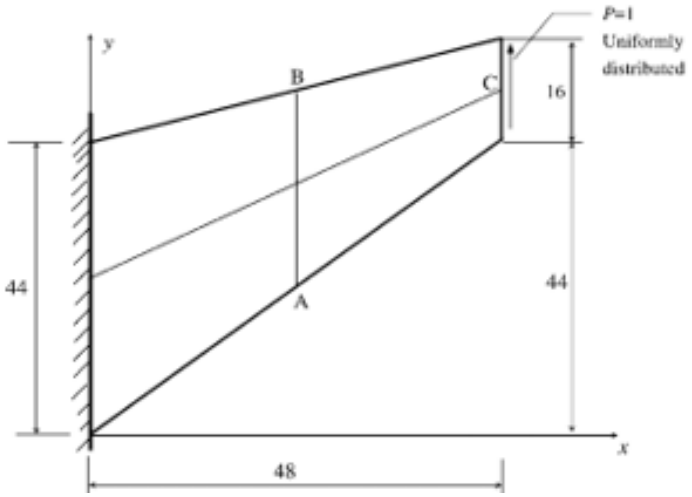

Fig. 7. Non-prismatic cantilever beam in reference Fu *et al.* (2010)

Table 6 Results of a non-prismatic cantilever beam

Element		v_C	$\sigma_{A.max}$	$\sigma_{B.min}$
Fu *et al.* (2010)	Q8(2×2)	22.72	0.2479	-0.2275
	Q8 (4×4)	23.71	0.2421	-0.2007
	Q8 (8×8)	23.88	0.2390	-0.2041
	Q9 (2×2)	23.29	-	-
	Q9 (4×4)	23.84	-	-
	Q9 (8×8)	23.94	-	-
	Q8α (2×2)	22.98	-	-
	Q8α (4×4)	23.74	-	-
	Q8α (8×8)	23.89	-	-
	AQ8-I/II (2×2)	22.98	0.2523	-0.2144
	AQ8-I/II (4×4)	23.74	0.2415	-0.2024
	AQ8-I/II (8×8)	23.89	0.2389	-0.2041
	QACM8 (2×2)	22.98	0.1959	-0.2142
	QACM8 (4×4)	23.74	0.2414	-0.2024
	QACM8 (8×8)	23.89	0.2389	-0.2041
	ATFQ8 (2×2)	23.80	0.2434	-0.1771
	ATFQ8 (4×4)	23.96	0.2404	-0.2049
	ATFQ8 (8×8)	23.96	0.2373	-0.2037
This study	AR8	22.20	0.2298	-0.2312
	AR20	23.96	0.2360	-0.2025
Exact		23.96	0.2362	-0.2023

7.6 Example 6

Fig. 7 demonstrates a non-prismatic cantilever beam, which is solved in this part. The shear load on the structural free edge is applied, according to Fig. 7 Fu *et al.* (2010). After performing numerical analyses, the obtained outcomes of vertical displacement at point C, maximum stress at point A and the minimum stress at point B are shown in Table 6. These responses are compared with the other available ones. The authors' element, AR20, gives very good answers against a variety of elements. In this example, E, μ and t are considered as 1.0, 0.333 and 1.0, respectively.

7.7 Example 7

A thin cantilever beam is used in this example, as it is shown in Fig. 8. In order to test the recommended elements for the sensitivity to the mesh shapes, three different mesh shapes are adopted, like a rectangular, parallelogram and trapezoidal Fu *et al.* (2010). In this example, pure bending and transverse linear load are applied. Beam's material has the following values. Young's modulus, Poisson's ratio and thickness are 10^7, 0.3 and 0.1, respectively. The obtained outcomes for this structure are given in Table 7. To illustrate the performance of the recommended elements, all findings are compared to each other. According to Table 7, it can be seen that the existing elements possess high accuracy for the rectangular element with 40 degrees of freedoms. Once more, the answers exhibit that the projected elements are capable of furnishing the exact solutions for the pure bending problem.

7.8. Example 8

Fig. 9 shows the bending of a thick curved beam with different meshes. This cantilever beam is subjected to a transverse force Fu *et al.* (2010). After analyzing this structure, the outcomes of the vertical displacements, at point A, are given in Table 8. Good performances are achieved from this study. In this example, the Poisson's ratio, modulus of elasticity and thickness are 0.0, 1000and 1.0, respectively.

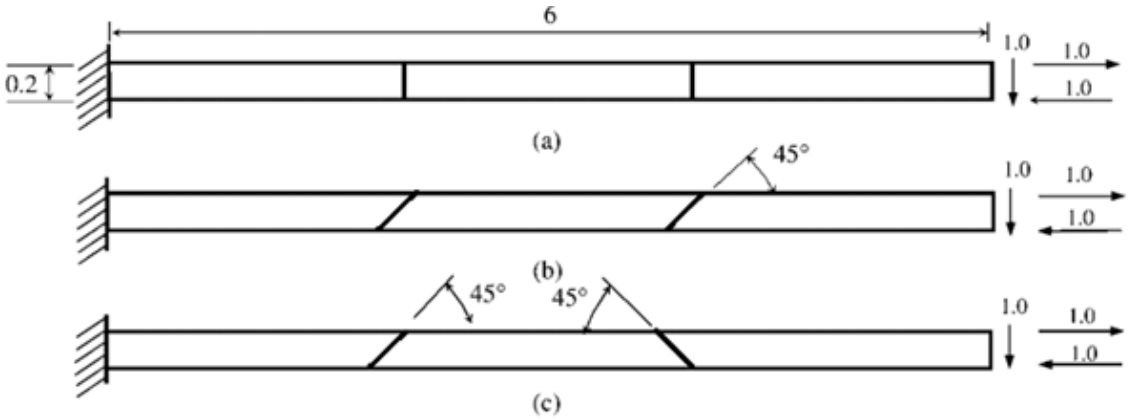

Fig. 8. A thin cantilever beam with different meshes

Table 7 Normalized displacement results for cantilever beam with different meshes

Element		Load P	Moment M
Fu *et al.* (2010)	Q8 (mesh a)	0.951	1.000
	Q8 (mesh b)	0.919	0.994
	Q8 (mesh c)	0.854	0.939
	QACM8 (mesh a)	0.951	1.000
	QACM8 (mesh b)	0.903	1.000
	QACM8 (mesh c)	0.895	1.000
	ATF-Q8 (mesh a)	0.978	1.000
	ATF-Q8 (mesh b)	0.968	1.000
	ATF-Q8 (mesh c)	0.996	1.000
This study	AR8	0.952	1.000
	AR20	0.998	1.000
Exact		1.000	1.000

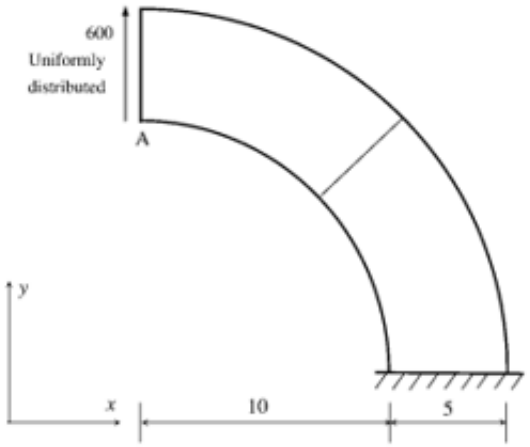

Fig. 9 Bending of a thick curved beam with different meshes according to Cen *et al.* (2012)

Table 8 The tip displacement of a thick curving beam with different meshes

Element		Displacement
Cen *et al.* (2012)	Q8 (1 × 1)	30.2
	Q8 (1 × 2)	77.4
	Q8 (1 × 4)	88.6
	QACM8 (1 × 1)	42.7
	QACM8 (1 × 2)	75.5
	QACM8 (1 × 4)	84.1
	ATF-Q8 (1 × 1)	56.5
	ATF-Q8 (1 × 2)	90.5
	ATF-Q8 (1 × 4)	90.4
This study	AR8	88.9
	AR20	90.2
Exact		90.1

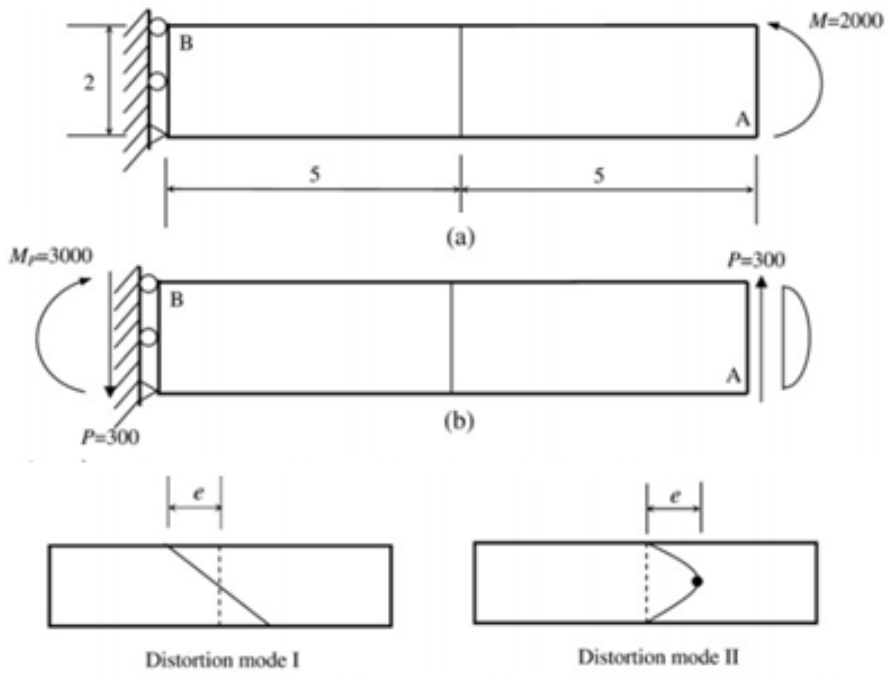

Fig. 10 Cantilever beam divided into different elements

As it is seen in Table 8, the presented elements can result in more accurate displacement outcomes for the curve members than previous elements proposed by the other researchers. Based on the obtained responses, the accuracy was raised by increasing the node numbers.

7.9 Example 9

In this example, a cantilever beam is meshed by different elements, as it is seen in Fig. 10. This problem is commonly used as a benchmark for testing the sensitivity to the mesh shapes Cen *et al.* (2012). To demonstrate the behavior of the new formulation, this structure is analyzed under the pure bending of M=2000, and the linear bending of P=150. It should be mentioned that the pure bending M is distributed as $f_x = -120y + 120$ and the linear bending P is distributed as $f_y = 75y - 37.5y^2$. Additionally, for $M_P = 3000$, which is distributed as $f_x = -180y + 180$. In this example, Poisson's ratio, modulus of elasticity and thickness are 0.25, 1500 and 1.0, respectively.

The obtained outcomes of the deflection at point A, and the stress σ_x at point B, are given in Tables 9 and 10. These results are compared with the deflection and the stress at the selected points of a cantilever beam using the distortion mode I and II according to reference Cen *et al.* (2012). Numerical outcomes in Table 10 indicate that AR20 with 40 degrees of freedom can reach the exact solutions for the pure bending case.

According to Table 9 and 10, the stress can be projected with high accuracy by sing AR20. It should be mentioned that the performance of the proposed elements in order to predict stress fields is better than the other achieved responses.

Table 9 Normalized results for cantilever beam Cen *et al.* (2012).

	e	0	0.5	1	2	3	4	4.9
subjected to a pure bending M: distortion mode I	Deflection at point A, exact $v_A = 100.0$							
	Q8	1.000	0.9996	0.9936	0.8939	0.5971	0.3201	0.1975
	QACM8	1.000	1.000	1.002	1.007	1.019	1.037	1.069
	ATF-Q8	1.000	1.000	1.000	1.000	1.000	1.000	1.000
	Stress at point B, exact σ_{xB}=-3.000							
	Q8	1.000	1.011	1.040	1.079	1.235	1.235	6.416
	QACM8	1.000	0.9890	0.9677	0.8655	0.8281	0.8281	0.7793
	ATF-Q8	1.000	1.000	1.000	1.000	1.000	1.000	1.000
subjected to a pure bending M: distortion mode II	Deflection at point A, exact $v_A = 100.0$							
	Q8	1.000	0.7448	0.4735	0.2486	0.1783	0.1457	0.1269
	QACM8	1.000	0.9819	0.9667	0.9450	0.9346	0.9364	0.9498
	ATF-Q8	1.000	0.9943	0.9786	0.9411	0.9163	0.9058	0.8991
	Stress at point B, exact σ_{xB}=-3.000							
	Q8	1.000	0.7000	0.4646	0.3402	0.3167	0.2998	0.2833
	QACM8	1.000	0.9624	0.9276	0.8653	0.8111	0.7635	0.7254
	ATF-Q8	1.000	0.8797	0.7750	0.6838	0.7008	0.7512	0.7957
subjected to a linear bending P: distortion mode I	Deflection at point A, exact $v_A = 102.6$							
	Q8	0.9765	0.9630	0.9298	0.7992	0.5478	0.3255	0.2222
	QACM8	0.9765	0.9698	0.9483	0.8830	0.8489	0.8421	0.8470
	ATF-Q8	0.9959	0.9919	0.9839	0.9697	0.9547	0.8946	0.6916
	Stress at point B, exact σ_{xB}=-4.500							
	Q8	0.9152	0.9251	0.9257	0.9221	0.9486	1.216	7.188
	QACM8	0.9152	0.9021	0.8585	0.7122	0.6120	0.5356	0.4681
	ATF-Q8	0.9468	0.9506	0.9521	0.9761	0.9860	0.9643	0.9321
subjected to a linear bending P: distortion mode II	Deflection at point A, exact $v_A = 102.6$							
	Q8	0.9765	0.7677	0.5199	0.3064	0.2379	0.2040	0.1832
	QACM8	0.9765	0.9493	0.9250	0.8850	0.8558	0.8382	0.8353
	ATF-Q8	0.9959	0.9953	0.9882	0.9696	0.9602	0.9596	0.9623
	Stress at point B, exact σ_{xB}=-4.500							
	Q8	0.9152	0.6994	0.5088	0.3830	0.3417	0.3110	0.2854
	QACM8	0.9152	0.8790	0.8456	0.7860	0.7344	0.6895	0.6537
	ATF-Q8	0.9468	0.9079	0.8758	0.8592	0.8848	0.9167	0.9404

Table 10 Normalized obtained results for cantilever beam in this study

	Element	Deflection at point A, exact $v_A = 100.0$	Stress at point B, exact σ_{xB}=-3.000
subjected to a pure bending M: distortion mode III	AR8	0.936	0.984
	AR20	1.000	1.000
	Element	Deflection at point A, exact $v_A = 102.6$	Stress at point B, exact σ_{xB}=-4.500
subjected to a linear bending P: distortion mode II	AR8	0.927	0.958
	AR20	1.000	1.000

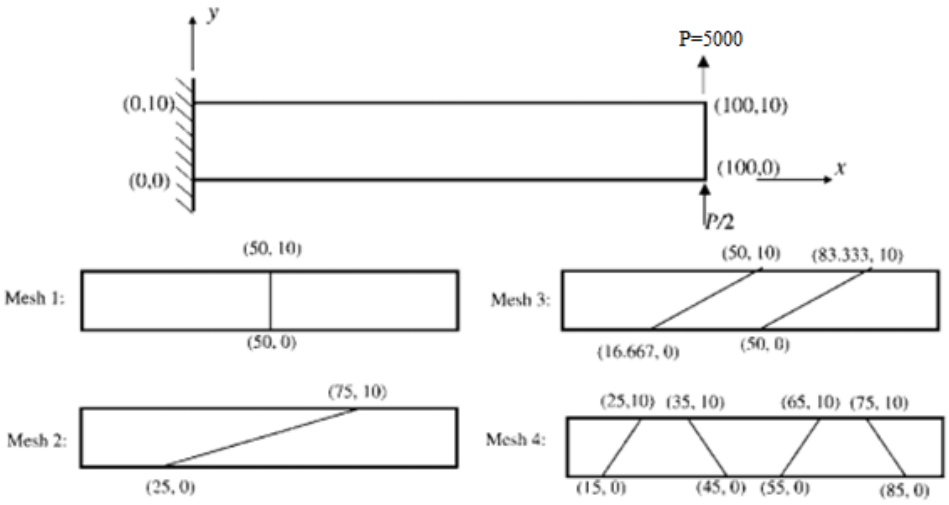

Fig. 11 Cantilever beam under linear bending with different meshes

7.10 Example 10

According to Fig. 11, a cantilever beam is displayed under linear bending. After analyzing this structure, the obtained outcomes of the deflection at the selected point are demonstrated in Table 11. The attained results show that AR20 has better performance than ATF-Q8 element. In this example, Poisson's ratio, modulus of elasticity and thickness are 0.30, 10^7 and 1.0, respectively.

As it is seen in Table 11, the consequences of displacement can be predicted by AR20 appropriately. These obtained answers are better than the previous methods.

8. Conclusion

In this study, a novel formulation for developing two stress based elements are proposed. All the suggested elements have rectangular shapes. According to comprehensive numerical studies, authors' formulas can solve the plane problem precisely. In fact, new elements give accurate responses for both displacement and stress. As it is demonstrated in the manuscript, the entire element construction procedure is different from those of the traditional models. Based on this study, the following results are achieved.

1. High-accuracy outcomes of the stress and displacement of complex curve members can be achieved by AR20.
2. Performances of AR20 in various meshes are better than those ones presented previously.
3. AR20 has high convergence speed in solving plane problems, since it uses fewer elements in the analyses process.
4. The accuracies of AR20 for finding the displacement values are higher than those obtained by using AR8.
5. The performances of AR8 for calculating the stress values are more precise than the obtained displacements.
6. Both proposed elements can analyze efficiently the problems having different load conditions.

Table 11 Responses of cantilever beam under linear bending

	Mesh	Elements	coordinate	displacement	Exact
(Cen *et al.* 2012)	1	Q8	$v(100.0)$	3.85	4.03
	2			0.74	
	3			2.00	
	4			3.65	
	1	Q9		3.86	
	2			3.18	
	3			3.34	
	4			3.98	
	1	Q8∝		3.85	
	2			3.16	
	3			3.32	
	4			3.967	
	1	L8		3.80	
	2			3.18	
	3			3.58	
	4			3.92	
This study	1	AQ8-I/II		3.85	
	2			3.15	
	3			3.30	
	4			3.99	
	1	ATF-Q8		3.89	
	2			3.45	
	3			3.94	
	4			4.00	
	5	AR8		3.82	
	6			3.85	
	7			3.90	
	8			3.97	
	5	AR20		3.89	
	6			3.92	
	7			4.00	
	8			4.04	

References

Albocher, U., Oberai, A.A., Barbone, P.E and Harari, I. (2009), "Adjoint-weighted equation for inverse problems of incompressible plane-stress elasticity", *Comput. Methods Appl. Mech. Eng.*, **198**(30–32), 2412-2420. https://doi.org/10.1016/j.cma.2009.02.034.

Bell, K. (1969), "A refined triangular plate bending element", *J. Numeric Methods Eng.*, **1**(1), 101–122. https://doi.org/10.1002/nme.1620010108.

Berry, M. V. and Balazs, N. L. (1979), "Nonspreading wave packets", *American J. Phys.,* **47**(3), 264–267. https://doi.org/10.1119/1.11855.

Cen, S., Zhou, M. J. and Fu, X. R. (2011a), "A 4-node hybrid stress-function (HS-F) plane element with drilling degrees of freedom less sensitive to severe mesh distortions", *Comput. Struct.*, **89**(5–6), 517-528. https://doi.org/10.1016/j.compstruc.2010.12.010.

Cen, S., Fu, X. R. and Zhou, M. J. (2011b), "8- and 12-node plane hybrid stress-function elements immune to severely distorted mesh containing elements with concave shapes", *Comput. Methods Appl. Mech. Eng.*, **200**(29-32), 2321–2336. https://doi.org/10.1016/j.cma.2011.04.014.

Cen, S., Fu, X. R., Zhou, G. H., Zhou, M. J. and Li, C. F. (2011c), "Shape-free finite element method: The plane hybrid stress-function (HS-F), element method for anisotropic materials", *Sci. China Phys., Mech. Astronomy*, **54**(4), 653–665. https://doi.org/10.1007/s11433-011-4272-6.

Chen, J., Li, C. J. and Chen, W. J. (2010), "A family of spline finite elements", *Comput. Struct.*, **88**(11-12), 718–727. https://doi.org/10.1016/j.compstruc.2010.02.011.

Cen, S., Chen, X. M. and Fu, X. R. (2007), "Quadrilateral membrane element family formulated by the quadrilateral area coordinate method", *Comput. Methods Appl. Mech. Eng.*, **196**(41-44), 4337-4353. https://doi.org/10.1016/j.cma.2007.05.004.

Chien, W. Z. (1980), *Calculus of Variations and Finite Elements (in Chinese)*, Science Press, Beijing.

Cen, S., Zhou, G. H. and Fu, X. R. (2012), "A shape-free 8-node plane element unsymmetric analytical trial function method", *J. Numerical Methods in Eng.*, **91**(2), 534-562. https://doi.org/10.1002/nme.4260.

Chen, X. M., Cen, S. and Long, Y. Q. (2004), "Membrane elements insensitive to distortion using the quadrilateral area coordinate method", *Comput. Struct.*, **82**(1), 35–54. https://doi.org/10.1016/j.compstruc.2003.08.004.

Fu, X. R., Cen, S., Li, C. F. and Chen, X. M. (2010), "Analytical trial function method for the development of new 8-node plane element based on the variational principle containing Airy stress function", *Eng. Comput.*, **27**(4), 442-463. https://doi.org/10.1108/02644401011044568.

Fernando, L., Muñoz, P. and Roehl, D. (2017), "An analytical solution for displacements due to reservoir compaction under arbitrary pressure changes", *Appl. Math. Modelling*, **52**, 145-159. https://doi.org/10.1016/j.apm.2017.06.023.

Fleck, N. A., Muller, G. M., Ashby, M. F. and Hutchinson, J. W. (1994), "Strain gradient plasticity: theory and experiment", *Acta Metallurgica et Materiali,* **42**(2), 475–487. https://doi.org/10.1016/0956-7151(94)90502-9.

Gao, Q. and Zou, M. Y. (2017), "An analytical solution for two and three dimensional nonlinear Burgers' equation", *Appl. Math. Modelling,* **45**, 255-270. https://doi.org/10.1016/j.apm.2016.12.018.

Hou, X., Lee, H. P., Ong, C. J. and Lim, S. P. (2016), "Shock analysis of a new ultrasonic motor subjected to half-sine acceleration pulses", *Adv. Comput. Design,* **1**(4), 357-370. http://dx.doi.org/10.12989/acd.2016.1.4.357.

Hutchinson, J. W. and Fleck, N.A. (1993), "A phenomenological theory for strain gradient effects in plasticity", *J. Mech. Phys. Solids,* **41**(12), 1825–1857. https://doi.org/10.1016/0022-5096(93)90072-N.

Hsu, Y. S. (2016), "Enriched finite element methods for Timoshenko beam free vibration analysis", *Appl. Math. Modelling*, **40**(15–16), 7012-7033. https://doi.org/10.1016/j.apm.2016.02.042.

Hu, H.C. (1984), *Variational Principles of Theory of Elasticity with Applications*, Science Press, Beijing.

Hirtum, A.V. (2017), "Quasi-analytical solution of two-dimensional Helmholtz equation", *Appl. Math. Modelling*, **47**, 96-102. https://doi.org/10.1016/j.apm.2017.03.026.

Haitao, C., Chen, Y. L. and Lu, Z. C. (2012), "Euler–Bernoulli beam under arbitrary dynamic loads", *J. Mech. Phys. Solids*, **57**, 1835-1867.

Koiter, W. T. (1969), "Couple stresses in the theory of elasticity I & II", *Philosophical Transactions Royal Society London B,* **67**, 17–44.

Li, L. X., Chen, Y. L. and Lu, Z. C. (2015), "Generalization of the multi-scale finite element method to plane elasticity problems", *Appl. Math. Modelling*, **39**(2), 642-653. https://doi.org/10.1016/j.apm.2014.06.012.

Li, C.J. and Wang, R.H. (2006), "A new 8-node quadrilateral spline finite element", *J. Computational Appl. Math.,* **195**(1-2), 54-65. https://doi.org/10.1016/j.cam.2005.07.017.

Lee, N.S. and Bathe, K.J. (1993), "Effects of element distortion on the performance of isoparametric elements", *J. Numeric Methods Eng.*, **36**(20), 3553–3576. https://doi.org/10.1002/nme.1620362009.

Long, Z.F., Li, J.X. and Cen, S. (1999), "Some basic formulae for area coordinates used in quadrilateral elements", *Communication Numerical Methods Eng. Banner*, **15**(12), 841–852. https://doi.org/10.1002/(SICI)1099-0887(199912)15:12<841::AID-CNM290>3.0.CO;2-A.

Luobin, L., Fuquan, C. and Zeng, C. (2019), "An analytical solution for sectional estimation of stress and displacement fields around a shallow tunnel", *Appl. Math. Modelling*, **69**, 181-200. https://doi.org/10.1016/j.apm.2018.12.012.

Madeo, A., Zagari, G. and Casciaro, R. (2012), "An isostatic quadrilateral membrane finite element with drilling rotations and no spurious modes", *Finite Elements in Analysis and Design*, **50**, 21-32. https://doi.org/10.1016/j.finel.2011.08.009.

Mindlin, R. D. (1964) "Microstructure in linear elasticity", *Archive for Rational Mechanics and Analysis,* **16**(1), 51–78. https://doi.org/10.1007/BF00248490.

Madeo, A., Casciaro, R., Zagari, G., Zinno, R. and Zucco, G. (2014), "A mixed isostatic 16 dof quadrilateral membrane element with drilling rotations based on Airy stresses", *Finite Elements in Analysis and Design*, **89**: 52-66. https://doi.org/10.1016/j.finel.2014.05.013.

Nix, W. D. and Gao, H. (1998) "Indentation size effects in crystalline materials: a law for strain gradient plasticity", *J. Mech. Phys. Solids,* **46**(3), 411–425. https://doi.org/10.1016/S0022-5096(97)00086-0.

Narwariya, M., Choudhury, A. and Sharma, A. K. (2018), "Harmonic analysis of moderately thick symmetric cross-ply laminated composite plate using FEM", *Adv. Comput. Design.* **3**(2), 113-132. http://dx.doi.org/10.12989/acd.2018.3.2.113.

Ooi, E. T., Rajendran, S. and Yeo, J. H. (2004), "A 20-node hexahedron element with enhanced distortion tolerance", *J. Numeric Methods Eng.*, **60**(15), 2501–2530. https://doi.org/10.1002/nme.1056.

Papanicolopulos, S. A. Zervos, A. and Vardoulakis, I. (2009), "A three dimensional C^1 finite the element for gradient elasticity", *J. Numeric Methods Eng.*, **77**(10), 1396–1415. https://doi.org/10.1002/nme.2449.

Rajendran, S. and Liew, K. M. (2003), "A novel unsymmetric 8-node plane element immune to mesh distortion under a quadratic displacement field", *J. Numeric Methods Eng.*, **58**(11), 1713-48. https://doi.org/10.1002/nme.836.

Rezaiee-Pajand, M. and Karimipour, A. (2019a), "Three stress‐based triangular elements", *Engineering with Computers* **20**(10), 1-12. https://doi.org/10.1007/s00366-019-00765-6.

Rezaiee-Pajand, M. and Karimipour, A (2019b), "Stress Analysis by Two Cuboid Isoparametric Elements", *European Journal of Computational Mechanics* **28**(5), 1-12. https://doi.org/10.13052/ejcm2642-2085.2851

Siviloglou, G. A. and Christodoulides, D. N. (2007), "Accelerating finite energy Airy beams", *Optics Letters,* **32**(8), 979–981. https://doi.org/10.1364/ol.32.000979.

Sergei, N., Viacheslav, K., Antti, B. and Niemi, H. (2016), "Variational formulation and isogeometric analysis for fourth-order boundary value problems of the gradient-elastic bar and plane strain/stress problems", *Comput. Methods Appl. Mech. Eng.*, **308**: 182-211. https://doi.org/10.1016/j.cma.2016.05.008.

Soh. A. K., Long. Y. Q. and Cen. S. (2000), "Development of eight-node quadrilateral membrane elements using the area coordinates method", *Computational Mechanics*, **25**(4), 376-84. https://doi.org/10.1007/s004660050484.

Stricklin, J.A., Ho, W.S., Richardson, E.Q. and Haister, W.E. (1977), "On isoparametric vs linear strain triangular elements", *J. Numeric Methods Eng.*, **11**(6), 1041-43. https://doi.org/10.1002/nme.1620110610.

Taylor, R. L., Beresford, P. J. and Wilson, E. L. (1976), "A non-conforming element for stress analysis", *J. Numeric Methods Eng.*, **10**(6), 1211–1219. https://doi.org/10.1002/nme.1620100602.

Toupin. R. A. (1962) "Elastic materials with couple stresses", *Archive for Rational Mechanics and Analysis,* **11**(1), 385–414. https://doi.org/ 10.1007/BF00253945.

Ushio, Y., Saruwatari, T. and Nagano, Y. (2019), "Elastoplastic FEM analysis of earthquake response for the field-bolt joints of a tower-crane mast", *Adv. Comput. Design*, **4**(1), 53-72. https://doi.org/10.12989/acd.2019.4.1.053.

Vini, M. H. and Daneshmand, S. (2019), "Investigation of bonding properties of Al/Cu bimetallic laminates fabricated by the asymmetric roll bonding techniques", *Adv. Comput. Design,* **4**(1), 33-41. http://doi.org/10.12989/acd.2019.4.1.033.

Willberg, C. (2016), "Analysis of the dynamical behavior of piezoceramic actuators using piezoelectric isogeometric finite elements", *Adv. Comput. Design*, **1**(1), 37-60. http://doi.org/10.12989/acd.2016.1.1.037.

Wei, Y. G., Wang, X. Z. and Wu, X. L. (2001), "Theoretical and experimental study on micro-indentation size effects (in Chinese)", *Science China (A),* **30**, 1025–1032. http://doi.org/10.1007/BF02872285.

Washizu, K. (1982), "*Variational Methods in Elasticity and Plasticity*", 3rd ed., Pergamon Press, New York, NY.

Yang, F., Chong, A. M., Lam, D. C. C. and Tong, P. (2002), "Couple stress based strain gradient theory for elasticity" *J. Solids Struct.,* **39**(10), 2731–2743. https://doi.org/10.1002/zamm.19840640121.

Zervos, A., Papanastasiou, P. and, Vardoulakis, I. (2001), "Modelling of localization and scale in thick-walled cylinders with gradient elastoplasticity", *J. Solids Struct.*, **38**(30-31), 5081–5095. https://doi.org/10.1016/S0020-7683(00)00337-1.

Zervos, A., Papanicolopulos, P. and Vardoulakis, I. (2009), "Two finite element discretization for gradient elasticity", *J. Eng. Mech.,* **135**(3), 203–213. https://doi.org/10.1061/(ASCE)0733-9399(2009)135:3(203).

Zhou, P. and Cen, S. (2015) "A novel shape-free plane quadratic polygonal hybrid stress-function element", *Math. Problems Eng.*, **2015**, 302-325. http://doi.org/10.1155/2015/491325.

Zienkiewicz, O. C., Taylor, R. L. and Zhu, J. Z. (2005), *The Finite Element Method: Its Basis & Fundamental*, 6th ed., Butterworth Heinemann, U.S.A.

Zhaolin, C., Zhichun, Y., Ning, G. and Guiwei, Z. (2018), "An energy finite element method for high-frequency vibration analysis of beams with axial force", *Appl. Math. Model.,* **61**, 521-539. https://doi.org/10.1016/j.apm.2018.04.016.

CC